Full-Vectorial Meshfree Finite Cloud Mode Solver for Fused Fiber-Optic Couplers

Xiaoer Wu[1,*] and Jinbiao Xiao[1]
[1]National Research Center for Optical Sensing/Communications Integrated Networking, School of Electronic Science and Engineering, Southeast University, Nanjing 210096, China
*Corresponding author, e-mail address: wuxiaoer512@163.com

***Abstract*—A novel full-vectorial meshfree finite cloud mode solver is proposed for analysis of fused optic-fiber couplers, in which the curvilinear coordinate mapping technique is used to map a cloud with curved interface onto a unit square. Numerical results are compared with prior analysis using the finite difference method, showing the validity and utility of the proposed method.**

I. Introduction

In the optical fiber systems, the fiber-optic couplers made by the fusing technology have been widely regarded as key building blocks to construct all-fiber devices, such as filters, powersplitter and multiplexers [1][2]. Accurate and low-cost simulation techniques play important roles in the analysis of their optical properties. Among them, the finite difference method (FDM) is attractive due to the advantages of simple implementation and universal application [3][4]. Its basis function, however, is usually low order, leading to large matrix. Recently, a meshfree finite cloud method (FCM) has attracted considerable attention due to its fast convergence and lower computational efforts and has been successfully applied to solve isotropic and anisotropic optical waveguides [5][6]. The FCM utilizes a fixed kernel approximation to construct a high-order meshfree interpolation basis function for keeping its high accuracy. Moreover, the FCM is suitable for analysis of complex material interfaces since the unconstraint nodes can be constructed in a completely free manner. Here, we apply the FCM scheme for full-vectorial analysis of fused fiber-optic couplers. To derive the full-vectorial formulations, the curvilinear coordinate mapping technique is adopted. Moreover, the cross-section of such coupler is divided into several clouds and then assembled by the interface boundary conditions. Numerical results show that the FCM can achieve the equivalent convergence with much less computational efforts.

II. Mathematical Formulations

Considering a fused fiber-optic coupler shown in Fig. 1, its cross-section is portioned into several uniform clouds. Then, for a single cloud, the coupled full-vectorial wave equations based on the electric field are given by

$$H_x^{(xx)}+\left(\varepsilon_r^{-1}\varepsilon_r^{(x)}H_x\right)^{(x)}+H_x^{(yy)}+k_0^2\varepsilon_r H_x+\left(\varepsilon_r^{-1}\varepsilon_r^{(y)}H_y\right)^{(x)}=\beta^2 H_x \quad (1a)$$

$$H_y^{(xx)}+\left(\varepsilon_r^{-1}\varepsilon_r^{(y)}H_y\right)^{(y)}+H_y^{(yy)}+k_0^2\varepsilon_r H_y+\left(\varepsilon_r^{-1}\varepsilon_r^{(x)}H_x\right)^{(y)}=\beta^2 H_y \quad (1b)$$

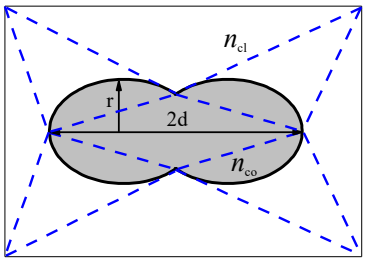

Fig. 1 Cross-section and sliced clouds of fused fiber-optic coupler.

where $\beta=k_0 n_{\text{eff}}$ with k_0 being the wave number in vacuum and n_{eff} being the effective refractive index. The superscripts (l) and (ll) denote the first and second derivatives with respect to l(l=x, y). To apply the formulations into clouds with curved interfaces, the coordinate mapping technique is introduced as follows:

$$H_x=\cos\varphi H_\rho-\sin\varphi H_\varphi \qquad H_y=\sin\varphi H_\rho+\cos\varphi H_\varphi \quad (2)$$

$$I^{(x)}=\cos\varphi I^{(\rho)}-\sin\varphi R^{-1}I^{(\varphi)} \qquad I^{(y)}=\sin\varphi I^{(\rho)}+\cos\varphi R^{-1}I^{(\varphi)} \quad (3)$$

where R is the effective radius and I is the unit vector. $(\rho,\ \varphi)$ denotes the curvilinear coordinates. Thus, the coupled full-vectorial eigenvalue equation is derived as follows:

$$\begin{bmatrix} T_{\rho\varphi} & T_{\rho\varphi} \\ T_{\rho\varphi} & T_{\rho\varphi} \end{bmatrix}\begin{bmatrix} a & -b \\ b & a \end{bmatrix}\begin{bmatrix} H_\rho \\ H_\varphi \end{bmatrix}=\beta^2\begin{bmatrix} a & -b \\ b & a \end{bmatrix}\begin{bmatrix} H_\rho \\ H_\varphi \end{bmatrix}. \quad (4)$$

where $a=\cos\varphi$, $b=\sin\varphi$ and

$$T_{\gamma\gamma}=I^{(\rho\rho)}+R^{-1}I^{(\rho)}+R^{-1}I^{(\varphi\varphi)}+k_0^2\varepsilon_r-\varepsilon_r^{-2}A_{\gamma\gamma}+\varepsilon_r^{-1}B_{\gamma\gamma}+\varepsilon_r^{-1}C_{\gamma\gamma} \quad (5a)$$

$$T_{\gamma\eta}=-\varepsilon_r^{-2}A_{\gamma\eta}+\varepsilon_r^{-1}B_{\gamma\eta}+\varepsilon_r^{-1}C_{\gamma\eta} \quad (5b)$$

where $\gamma,\eta=\rho,\varphi$ and

$$A_{\rho\rho}=a^2\varepsilon_r^{(\rho)2}-2abR^{-1}\varepsilon_r^{(\rho)}\varepsilon_r^{(\varphi)}+b^2\varepsilon_r^{(\varphi)2} \quad (6a)$$

$$B_{\rho\rho}=a^2\varepsilon_r^{(\rho)2}-2bR^{-1}(a\varepsilon_r^{(\rho\rho)}+a\varepsilon_r^{(\varphi\varphi)}-b\varepsilon_r^{(\rho)}-bR^{-1}\varepsilon_r^{(\varphi\varphi)})+abR^{-2}\varepsilon_r^{(\varphi)} \quad (6b)$$

$$C_{\rho\rho}=a\varepsilon_r^{(\rho)}(I\cdot)^{(\rho)}(\varepsilon_r^{(\rho)}+abR^{-1}\varepsilon_r^{(\varphi)})-abR^{-1}(I\cdot)^{(\varphi)}(a\varepsilon_r^{(\rho)}+bR^{-1}\varepsilon_r^{(\varphi)}) \quad (6c)$$

$$A_{\rho\varphi}=A_{\varphi\rho}=ab\varepsilon_r^{(\rho)2}+(a^2-b^2)R^{-1}\varepsilon_r^{(\rho)}\varepsilon_r^{(\varphi)}-abR^{-2}\varepsilon_r^{(\varphi)2} \quad (7a)$$

$$B_{\rho\varphi}=ab\varepsilon_r^{(\rho)2}+(a^2-b^2)R^{-2}\varepsilon_r^{(\rho\varphi)}-bR^{-1}[(a\varepsilon_r^{(\rho)}-b\varepsilon_r^{(\varphi)})+R^{-1}(b\varepsilon_r^{(\varphi)}-a\varepsilon_r^{(\varphi\varphi)})] \quad (7b)$$

$$C_{\rho\varphi}=ab\varepsilon_r^{(\rho)}(I\cdot)^{(\rho)}-b^2R^{-1}\varepsilon_r^{(\rho)}(I\cdot)^{(\varphi)}+aR^{-1}(I\cdot)^{(\rho)}(a\varepsilon_r^{(\varphi)}-b\varepsilon_r^{(\rho)}) \quad (7c)$$

$$B_{\varphi\rho}=ab\varepsilon_r^{(\rho)2}-bR^{-1}(b\varepsilon_r^{(\rho\varphi)}-a\varepsilon_r^{(\rho)}-aR^{-1}\varepsilon_r^{(\varphi\varphi)})+(a^2-b^2)R^{-1}(\varepsilon_r^{(\varphi)}-R^{-1}\varepsilon_r^{(\varphi)}) \quad (8a)$$

$$C_{\varphi\rho}=b(I\cdot)^{(\rho)}(a\varepsilon_r^{(\rho)}-b\varepsilon_r^{(\varphi)})+(I\cdot)^{(\varphi)}[(a^2-b^2)\varepsilon_r^{(\rho)}-abR^{-2}\varepsilon_r^{(\varphi)}] \quad (8b)$$

$$A_{\rho\rho}=b^2\varepsilon_r^{(\rho)2}+2abR^{-1}\varepsilon_r^{(\rho)}\varepsilon_r^{(\varphi)}+a^2\varepsilon_r^{(\varphi)2} \quad (9a)$$

$$B_{\varphi\varphi}=b^2\varepsilon_r^{(\rho)2}-2bR^{-1}(a\varepsilon_r^{(\rho\varphi)}+a\varepsilon_r^{(\varphi\varphi)}-\varepsilon_r^{(\varphi)})+a^2R^{-1}(\varepsilon_r^{(\varphi)}+R^{-1}\varepsilon_r^{(\varphi)2}) \quad (9b)$$

$$C_{\varphi\varphi}=b\varepsilon_r^{(\rho)}(I\cdot)^{(\rho)}(b\varepsilon_r^{(\rho)}+aR^{-1}\varepsilon_r^{(\varphi)})+aR^{-1}(I\cdot)^{(\varphi)}(b\varepsilon_r^{(\rho)}+aR^{-1}\varepsilon_r^{(\varphi)}) \quad (9c)$$

The unknown field components H_ρ and H_φ are expanded by a

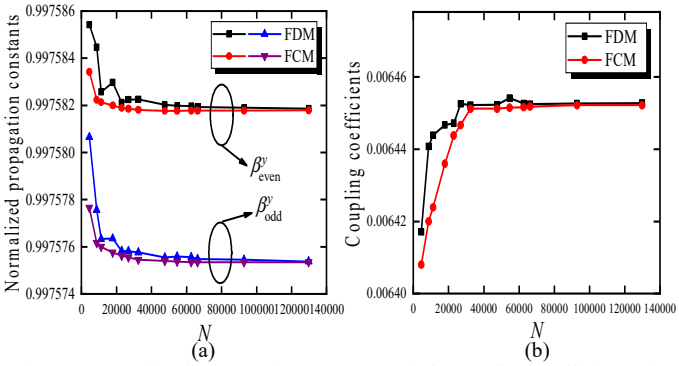

Fig.2 (a) Normalized propagation constants and (b) coupling coefficients of the *y*-polarized modes for the fused fiber-optic coupler.

fixed kernel shape function

$$H_\rho(\rho_i,\varphi_j)=\sum_{l=1}^{N_{in}} N_l(\rho_i,\varphi_j)H_{\rho l},\ H_\varphi(\rho_i,\varphi_j)=\sum_{l=1}^{N_{in}} N_l(\rho_i,\varphi_j)H_{\varphi l} \quad (10)$$

where (ρ_i,φ_j) is an arbitrary interior node in the cloud. $i=1,2,\cdots,N_\rho$ and $j=1,2,\cdots,N_\varphi$ with N_ρ being the transverse nodal number along the ρ axis and N_φ being the vertical nodal number along the φ axis. Therefore, the interior nodal number is denoted as $N_{in}=N_\rho\times N_\varphi$. Substituting (10) into (4), the eigenvalue equation for a single cloud can be derived.

After that, the boundary nodes shared by the adjacent clouds *a* and *b* are replaced by the following boundary conditions:

$$H_\varphi^{(\varphi)a}=H_\varphi^{(\varphi)b} \text{ and } H_\rho^{(\rho)a}=H_\rho^{(\rho)b}+(1-\varepsilon_r^{a-b})R^{-1}H_\rho^b, \quad (11a)$$

$$H_\rho^{(\varphi)a}=\varepsilon_r^{b-a}H_\rho^{(\varphi)b} \text{ and } H_\varphi^{(\rho)a}=H_\varphi^{(\rho)b}+(\varepsilon_r^{b-a}-1)R^{-1}H_\varphi^{(\rho)b}. \quad (11b)$$

By assembling all the clouds, we have

$$\begin{bmatrix} A_1 & \cdots & 0 \\ \vdots & \ddots & \vdots \\ 0 & \cdots & A_s \end{bmatrix}\begin{bmatrix} H^1 \\ \vdots \\ H^s \end{bmatrix}=\beta^2\begin{bmatrix} H^1 \\ \vdots \\ H^s \end{bmatrix} \quad (12)$$

where A_v and $H^v=\begin{bmatrix} H_\rho^v & H_\varphi^v \end{bmatrix}^T (v=1,2,\cdots,s)$ denote the eigenvalue equation for a single cloud and the values of H_ρ and H_ϕ at the interpolated nodes of the *i*th clouds, respectively.

III. Numerical Results and Discussion

In this numerical experiment, the computational window is taken as $28\mu m\times 28\mu m$. The refractive indexes of the core and cladding layers are $n_{co}=1.45$, $n_{cl}=1.0$, respectively. The operating wavelength is set to be $\lambda=1.53\mu m$. The aspect ratio is $2d/2r=1.8$ with *r* being the radius of the individual core. In addition, the considered normalized frequency is taken as $V=(2\pi/\lambda)\cdot r\cdot(n_{co}^2-n_{cl}^2)^{0.5}=50$. These parameters are the same as those used in [4]. In order to verify the convergent behavior of the proposed FCM mode solver, the normalized propagation constants of the lowest-order even and odd modes of *y* polarization are presented in Fig. 2(a), in which the expression of the normalized propagation constant is defined by $\beta'=(n_{co}\beta-n_{cl}k_0)/(n_{co}k_0-n_{cl}k_0)$. In order to make comparison more intuitive, results obtained by the FDM [4] are also plotted in the same figure. The convergent solutions of the two modes calculated by the FDM are $\beta^y_{even}=0.997581862\mu m^{-1}$

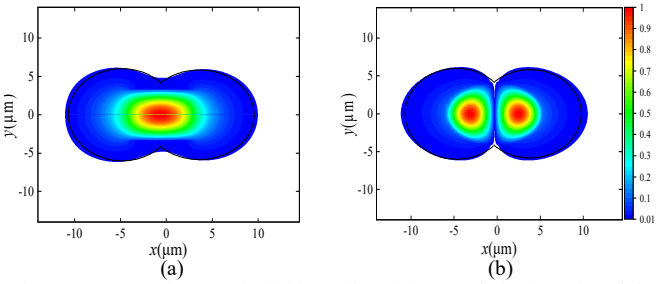

Fig. 3 Contours of magnetic field profiles of the *y*-polarized modes of the fused fiber-optic coupler: (a) even mode and (b) odd mode.

and $\beta^y_{odd}=0.997575478\mu m^{-1}$. It can be seen that our results are in good agreement with those from the FDM. Moreover, the proposed FCM shows superior convergence to the FDM since the former with 35000 nodes can obtain convergent results than the latter with more than 60000 nodes. Fig. 2(b) shows the coupling coefficients of the *y*-polarized modes, in which the coupling coefficient of the *y* polarization state is defined as $rC_y=0.5\cdot r\cdot(\beta^y_{even}-\beta^y_{odd})$. It can be seen that results obtained by the FCM agree well with those by the FDM. However, the FDM requires more computational efforts than the proposed FCM since the FDM need more nodes to obtain a convergent value. Therefore, the FCM is more efficient. Fig. 3 shows the contours of magnetic field profiles of the *y*-polarized even and odd modes of the fused fiber-optic coupler.

IV. Conclusion

A novel full-vectorial meshfree finite cloud mode solver is developed for analysis of the fused fiber-optic couplers. Numerical results of normalized propagation constants and coupling coefficients accord well with those from the FDM, which validates the effectiveness of the FCM.

Acknowledgment

This work was supported by National Natural Science Foundation of China under Grants 11574046 and Natural Science Foundation of Jiangsu Province under Grant BK20211163.

References

[1] E. Pone, X. Daxhelet and S. Lacroix, "Refractive index profile of fused-fiber couplers cross-section," *Opt. Exp.*, vol. 12, no. 6, pp. 1036-1044, Mar. 2004.

[2] S. W. Yang and H. C. Chang, "Numerical modeling of weakly fused fiber-optic polarization beamsplitters-part I: accurate calculation of coupling coefficients and form birefringence," *J. Lightw. Technol.*, vol. 16, no. 4, pp. 685-690, Apr. 1998.

[3] J. Xiao and X. Sun, "Vector analysis of bending waveguides by using a modified finite-difference method in a local cylindrical coordinate system," *Opt. Exp.*, vol. 20, no. 19, pp. 21583-21597, Sep. 2012.

[4] Y. C. Chiang, Y. P. Chiou and H. C. Chang, "Improved full-vectorial finite-difference mode solver for optical waveguides with step-index profiles," *J. Lightw. Technol.*, vol. 20, no. 8, pp. 1609-1618, Aug. 2002.

[5] D. R. Burke and T. J. Smy, "Optical mode solving for complex waveguides using a finite cloud method," *Opt. Exp.*, vol. 20, no. 16, pp. 17738-17751, Jul. 2012.

[6] X. Wu and J. Xiao, "Full-vectorial meshless finite cloud method for an anisotropic optical waveguide analysis," *Opt. Exp.*, vol. 29, no. 22/25, pp. 35271-35287, Oct. 2021.